Travelling waves in a model of quasi-active dendrites with active spines

Y Timofeeva*

Department of Computer Science and Centre for Complexity Science, University of Warwick, Coventry, CV4 7AL, UK

Abstract

Dendrites, the major components of neurons, have many different types of branching structures and are involved in receiving and integrating thousands of synaptic inputs from other neurons. Dendritic spines with excitable channels can be present in large densities on the dendrites of many cells. The recently proposed Spike-Diffuse-Spike (SDS) model that is described by a system of point hot-spots (with an integrate-and-fire process) embedded throughout a passive tree has been shown to provide a reasonable caricature of a dendritic tree with supra-threshold dynamics. Interestingly, real dendrites equipped with voltage-gated ion channels can exhibit not only supra-threshold responses, but also sub-threshold dynamics. This sub-threshold resonant-like oscillatory behaviour has already been shown to be adequately described by a quasi-active membrane. In this paper we introduce a mathematical model of a branched dendritic tree based upon a generalisation of the SDS model where the active spines are assumed to be distributed along a quasi-active dendritic structure. We demonstrate how solitary and periodic travelling wave solutions can be constructed for both continuous and discrete spine distributions. In both cases the speed of such waves is calculated as a function of system parameters. We also illustrate that the model can be naturally generalised to an arbitrary branched dendritic geometry whilst remaining computationally simple. The spatio-temporal patterns of neuronal activity are shown to be significantly influenced by the properties of the quasi-active membrane. Active (sub- and supra-threshold) properties of dendrites are known to vary considerably among cell types and animal species, and this theoretical framework can be used in studying the combined role of complex dendritic morphologies and active conductances in rich neuronal dynamics.

*y.timofeeva@warwick.ac.uk

I. INTRODUCTION

Dendrites with their complex, branching structures form the major receiving part on neural cells and represent the targets for synaptic inputs from other neurons. Ramón y Cajal who was one of the first to investigate the structure of the central nervous system more than 100 years ago revealed that dendritic spines are present in the dendrites of many neurons of the cerebral cortex of mammals [1]. Dendritic spines are small protrusions from the dendrites (usually no more than 2 μm) with a bulbous head attached to the dendrite by a narrow stem, and they are frequently found on the dendrites of many types of neurons. Interestingly, different dendrites of a given neuron may exhibit widely different spine densities and such variations may even be observed along the length of a dendritic segment. Dendritic spines are the most common synaptic specialisations that provide junction points for the axons of other neurons and have been linked to a basic mechanism for Hebbian learning in the nervous system [2]. The properties of spines have been also associated with the amplification of distal synaptic inputs [3], orientation tuning in complex cells of the visual cortex [4], coincidence detection [5] and the implementation of logical computations [6]. Recent advances in molecular tools and imaging methods additionally reveal that together with complex electro-chemical changes spines might undergo morphological changes, thereby linking dendritic spines to neuronal plasticity and long-term memory formation [7, 8]. Moreover, confocal and two-photon microscopy observations have confirmed the generation of action potentials in the dendrites [9], and dendritic spines equipped with excitable membranes provide favorable sites for initiations of these action potentials.

One of the first theoretical models of spiny dendritic tissue was proposed by Baer and Rinzel [10] who considered a passive uniform unbranched dendritic cable coupled to a population of excitable dendritic spines. In this *continuum* model the spines are coupled to the dendrite via a spine stem resistance and the active spine-head dynamics is described by Hodgkin-Huxley kinetics. Numerical simulations have shown that global signals, in the form of travelling pulses [10] as well as periodic and irregular travelling waves [11], may be supported by this system. Later, Coombes and Bressloff showed that the active membrane dynamics of spines could be analytically treated using an integrate-and-fire (IF) process [12] (instead of Hodgkin-Huxley kinetics). The resulting Spike-Diffuse-Spike

(SDS) model is an idealised system for the description of dendritic wave propagation in spine-studded dendritic trees, and importantly it admits exact mathematical analysis. This reduced model has been extensively studied with both continuous and discrete distributions of active spines, and has been shown to support solitary pulses, periodic travelling waves and irregular wave patterns [12–16]. In all these studies the dendrites are considered to be purely passive. This assumption does not account for voltage-gated ion channels that are present in dendrites of many neurons (see [17] for a recent review), and in particular those that can exhibit sub-threshold oscillatory behaviour and resonances (for example, Ca^{2+}-activated K^+ and hyperpolarisation-activated (h) channels). The channels associated with the I_h current especially have received considerable attention from experimentalists in recent years after being discovered at extremely high densities in distal dendrites of CA1 (a layer of hippocampus) and cortical pyramidal neurons. These channels have been shown to have a large impact on the integration of synaptic activity [18]. From a mathematical perspective Hodgkin and Huxley in their classical work of 1952 [19] and later Mauro *et al.* [20] have demonstrated that a linearisation of such channel kinetics around the steady-state may adequately describe the observed resonant dynamics. This is also supported by the recent finding that under sub-threshold conditions dendritic processing of time-varying inputs in cortical and hippocampal pyramidal neurons can be described as a linear filter [21, 22]. The linear approximation extends the more usual 'RC' circuit description of a passive membrane to the so-called quasi-active case (modelled by an 'LRC' circuit) that is able to display resonant-like behaviour due to the additional presence of inductances [23].

In this paper a generalised version of the SDS model is introduced and studied where the active spines are distributed along a resonant (rather than a passive) dendritic structure. In Section II we provide the general form of the model with the dynamics of a dendritic cable described by a quasi-active membrane. Next, in Section III we consider the continuum limit of this model where spines are uniformly distributed along the cable. We demonstrate how the profiles of solitary pulse, double pulse and periodic travelling wave solutions can be explicitly constructed in this model and how the speed of such travelling waves can be studied as a function of system parameters. In Section IV we consider a more biologically realistic case of a discrete distribution of active spines and show how this model can be solved in terms of the Green's function of the infinite resonant dendrite.

We also study the speed of the corresponding saltatory travelling wave as a function of spine spacing. In Section V we generalise the discrete model of Section IV to an arbitrary dendritic geometry. The voltage response across the branching structure is constructed using the "sum-over-trips" techniques for dendrites with a quasi-active membrane recently developed by Coombes *et al.* [24] as a generalisation of the original work of Abbott *et al.* [25] for passive dendrites. This approach obviates the need for the numerical solution of an underlying set of partial differential equations (PDEs) and leads to a minimal computationally fast model of dendrites with active channels which can regulate local spike initiations (e.g., Na^+, Ca^{2+} and K^+ channels) and sub-threshold resonance properties of neurons (e.g., Ca^{2+}-activated K^+ and h channels). In Section VI we provide a discussion of the further potential of this work.

II. THE MODEL

We consider an infinite unbranched dendritic cable with a resonant membrane and a given distribution of spines along its length (see schematic diagram in Figure 1). The dynamics of the membrane voltage in the cable $V = V(x,t)$ is described by the system of equations

$$\frac{\partial V}{\partial t} = D\frac{\partial^2 V}{\partial x^2} - \frac{V}{\tau} - \frac{1}{C}\left[I - \rho(x)\frac{\widehat{V} - V}{r_s}\right], \qquad x \in \mathbb{R}, \qquad t \in \mathbb{R}^+ \tag{1}$$

$$L\frac{\mathrm{d}I}{\mathrm{d}t} = -rI + V. \tag{2}$$

Here C is the capacitance of the cell membrane, $\tau = CR$ is the (passive) membrane time constant and D is the cable diffusion coefficient. The standard cable equation is coupled to a resonant current that flows through the path represented by an inductance L in series with a resistance r in an 'LRC' electrical circuit. Spines with the given distribution $\rho(x)$ are connected to the dendrite through the spine-stem resistance r_s and generate a sequence of action potentials in their spine heads given by the function $\widehat{V}(x,t)$. Denoting the mth firing time of the spine at position x by $T^m(x)$ we model

$$\widehat{V}(x,t) = \sum_m \eta(t - T^m(x)), \tag{3}$$

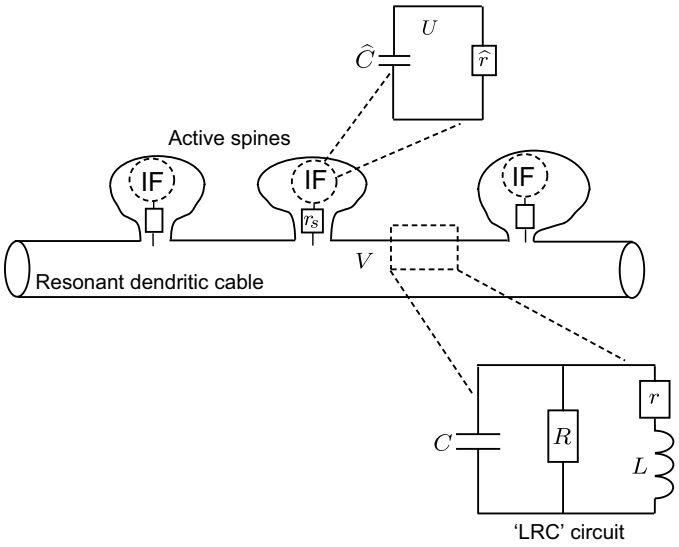

FIG. 1. Schematic diagram of a dendritic cable with resonant membrane and active spines.

where $\eta(t)$ specifies the universal shape of an action potential. These firing times are generated by an IF-type firing mechanism:

$$T^m(x) = \inf\{t \mid U(x,t) \geq h,\ t \geq T^{m-1}(x) + \tau_R\}. \tag{4}$$

The function $U(x,t)$ that plays the role of the generator of action potentials in spine heads evolves according to

$$\widehat{C}\frac{\partial U}{\partial t} = -\frac{U}{\widehat{r}} + \frac{V-U}{r_s}, \tag{5}$$

subject to the reset condition $U(x,t^+) = U_{\rm res}$ whenever $U(x,t)$ reaches the threshold level h, with $U_{\rm res} < h$. The parameters $\widehat{C}$ and $\widehat{r}$ describe the capacitance and resistance of the spine-head membrane respectively. Throughout the paper we consider a simple action potential shape given by a rectangular pulse $\eta(t) = \eta_0\Theta(t)\Theta(\tau_s - t)$ with strength η_0 and duration τ_s. Here $\Theta(t)$ is the Heaviside step function. The term τ_R in (4) represents a refractory timescale for controlling multiple spiking events from active spines and $\tau_R \geq \tau_s$. The model presented here can be easily reduced to the original SDS model (with a passive dendritic cable) [12–16] by considering the limit $r \to \infty$ for the resistance in the 'LRC' circuit.

III. CONTINUUM LIMIT

In this section we consider a constant spine distribution, i.e. $\rho(x) = \rho$ for all x, and show how one may explicitly construct the profiles of solitary and periodic travelling waves. We consider the firing time ansatz of a Δ periodic travelling wave as $T^m(x) = x/s + (m-1)\Delta$, where s denotes the speed of the wave and $m = 1, 2, \ldots$ A solitary wave that causes the spine head at x to reach threshold only once may then be described by the firing time $T^1(x) = x/s$. Introducing a moving frame $\xi = t - x/s$ travelling wave solutions of (1)–(2) satisfy:

$$\frac{D}{s^2}V_{\xi\xi} - V_\xi - \left(\frac{1}{\tau} + \frac{\rho}{Cr_s}\right)V - \frac{I}{C} + \frac{\rho\eta_0}{Cr_s}\Theta(\xi)\Theta(\tau_s - \xi) = 0, \tag{6}$$

$$LI_\xi = -rI + V, \tag{7}$$

where $V_\xi \equiv \mathrm{d}V/\mathrm{d}\xi$ and $I_\xi \equiv \mathrm{d}I/\mathrm{d}\xi$. The characteristic equation of the system of differential equations (6)–(7) describes solutions of the form $\mathrm{e}^{\lambda\xi}$ for the homogeneous problem and has the form

$$\lambda^3 + \left[\frac{r}{L} - \frac{s^2}{D}\right]\lambda^2 - \frac{s^2}{D}\left[\frac{r}{L} + \left(\frac{1}{\tau} + \frac{\rho}{Cr_s}\right)\right]\lambda - \frac{s^2}{DL}\left[\left(\frac{1}{\tau} + \frac{\rho}{Cr_s}\right)r + \frac{1}{C}\right] = 0. \tag{8}$$

It can be easily shown that the roots of this cubic polynomial, λ_i, $i = 1, \ldots, 3$, are restricted to the following two cases:

Case I) $\lambda_1 \in \mathbb{R}^+,\ \lambda_{2,3} \in \mathbb{R}^-$,

Case II) $\lambda_1 \in \mathbb{R}^+,\ \lambda_{2,3} = \alpha \pm \mathrm{i}\beta \in \mathbb{C},\ \alpha \in \mathbb{R}^-$.

For travelling pulse solutions which approach zero in the limit $\xi \to \pm\infty$ and when all $\lambda_i \in \mathbb{R}$ (i.e. Case I) the solution to (6)–(7) takes the form

$$I(\xi) = \begin{cases} c_1\mathrm{e}^{\lambda_1\xi}, & -\infty < \xi \le 0, \\ c_2\mathrm{e}^{\lambda_1\xi} + c_3\mathrm{e}^{\lambda_2\xi} + c_4\mathrm{e}^{\lambda_3\xi} + Q, & 0 \le \xi \le \tau_s, \\ c_5\mathrm{e}^{\lambda_2\xi} + c_6\mathrm{e}^{\lambda_3\xi}, & \xi \ge \tau_s, \end{cases} \tag{9}$$

$$V(\xi) = LI_\xi(\xi) + rI(\xi), \tag{10}$$

where

$$Q = \rho\eta_0\left[r_s\left(\left(\frac{1}{\tau} + \frac{\rho}{Cr_s}\right)rC + 1\right)\right]^{-1}.$$

By ensuring the continuity of $I(\xi)$, $V(\xi)$ and $V_\xi(\xi)$ at $\xi = 0$ and $\xi = \tau_s$ the unknown coefficients $c_1, \ldots, c_6$ may be found as follows

$$
\begin{aligned}
c_1 &= c_3 \frac{\lambda_2(\lambda_3 - \lambda_2)}{\lambda_1(\lambda_3 - \lambda_1)} (1 - \mathrm{e}^{-\lambda_1 \tau_s}), & c_2 &= -c_3 \frac{\lambda_2(\lambda_3 - \lambda_2)}{\lambda_1(\lambda_3 - \lambda_1)} \mathrm{e}^{-\lambda_1 \tau_s}, \\
c_3 &= Q \frac{\lambda_1 \lambda_3}{(\lambda_2 - \lambda_1)(\lambda_3 - \lambda_2)}, & c_4 &= -c_3 \frac{\lambda_2(\lambda_2 - \lambda_1)}{\lambda_3(\lambda_3 - \lambda_1)}, \\
c_5 &= c_3(1 - \mathrm{e}^{-\lambda_2 \tau_s}), & c_6 &= -c_3 \frac{\lambda_2(\lambda_2 - \lambda_1)}{\lambda_3(\lambda_3 - \lambda_1)} (1 - \mathrm{e}^{-\lambda_3 \tau_s}).
\end{aligned}
$$

If two roots of polynomial (8) are complex (i.e. λ_i satisfy Case II) the solution for $I(\xi)$ has the form

$$
I(\xi) = \begin{cases} \overline{c}_1 \mathrm{e}^{\lambda_1 \xi}, & -\infty < \xi \leq 0, \\ \overline{c}_2 \mathrm{e}^{\lambda_1 \xi} + \mathrm{e}^{\alpha \xi} [\overline{c}_3 \cos(\beta \xi) + \overline{c}_4 \sin(\beta \xi)] + Q, & 0 \leq \xi \leq \tau_s, \\ \mathrm{e}^{\alpha \xi} [\overline{c}_5 \cos(\beta \xi) + \overline{c}_6 \sin(\beta \xi)], & \xi \geq \tau_s, \end{cases} \tag{11}
$$

and the coefficients $\overline{c}_1, \ldots, \overline{c}_6$ may also be found from the continuity conditions (see Appendix A1 for more details). Two examples of the exact solutions for travelling pulses are shown in Figure 2.

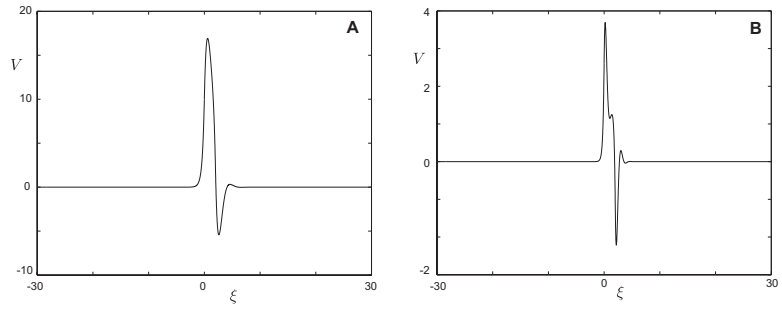

FIG. 2. The exact solutions for travelling pulses in the model of a resonant cable with active spines for the following parameters: $C = 1$, $\tau = 1$, $D = 1$, $r_s = 10$, $\eta_0 = 100$, $\tau_s = 2$, $\rho = 15$, $s = 1$, (**A**) $r = 0.1$, $L = 0.1$ and (**B**) $r = 0.01$, $L = 0.01$.

The self-consistent speed of the travelling pulse can be found along the lines outlined in [12] for the SDS model with a passive cable by demanding that the IF process in the spine head reaches the threshold h at $\xi = 0$. In the travelling wave frame the dynamics for the IF process has the form

$$
U_\xi = -\varepsilon_0 U + \frac{V}{\widehat{C} r_s}, \tag{12}
$$

where $\varepsilon_0 = (1/\widehat{r}+1/r_s)/\widehat{C}$. Solving this first-order system with the conditions $\lim_{\xi\to-\infty} U(\xi) = 0$ and $U(0) = h$ we get that

$$h = \frac{1}{\widehat{C}r_s}\int_{-\infty}^{0} V(\xi')\mathrm{e}^{\varepsilon_0\xi'}\mathrm{d}\xi'. \tag{13}$$

This yields an implicit equation for the speed of the pulse as a function of the system parameters:

$$h = q\frac{(L\lambda_1 + r)}{\widehat{C}r_s(\lambda_1 + \varepsilon_0)}, \tag{14}$$

where $q = c_1$ for Case I and $q = \overline{c}_1$ for Case II. This expression can be solved numerically for s. An example in Figure 3 (middle plot) demonstrates the speed of a travelling pulse as a function of the spine density ρ. Different curves demonstrate how the speed varies for the different choices of parameters r and L. An application of a linear stability analysis presented in [12] to this model as well as direct numerical simulations indicate that it is the faster branch that is stable. The resonant properties of a dendritic membrane have a noticeable impact on the minimum spine density capable of supporting a travelling pulse in the model. Four smaller plots in Figure 3 indicated by (a), (b), (c), and (d) show the examples of profiles of the stable travelling pulses for the parameters marked by crosses on the corresponding speed curves. Note that the speed curve (a) and the corresponding profile of a pulse are obtained in the limit $r \to \infty$ that recovers the results obtained in [12] for a passive dendritic membrane.

The propagation of a double pulse can be studied along the same lines by assuming an occurrence of two firing events from the spine head at position x at the firing times $T^1(x) = x/s$ and $T^2(x) = x/s + \Delta$. In this case the solution to equations (6)–(7) with real λ_i (Case I) takes the form

$$I(\xi) = \begin{cases} c_1\mathrm{e}^{\lambda_1\xi}, & -\infty < \xi \le 0, \\ c_2\mathrm{e}^{\lambda_1\xi} + c_3\mathrm{e}^{\lambda_2\xi} + c_4\mathrm{e}^{\lambda_3\xi} + Q, & 0 \le \xi \le \tau_s, \\ c_5\mathrm{e}^{\lambda_1\xi} + c_6\mathrm{e}^{\lambda_2\xi} + c_7\mathrm{e}^{\lambda_3\xi}, & \tau_s \le \xi \le \Delta, \\ c_8\mathrm{e}^{\lambda_1\xi} + c_9\mathrm{e}^{\lambda_2\xi} + c_{10}\mathrm{e}^{\lambda_3\xi} + Q, & \Delta \le \xi \le \Delta + \tau_s, \\ c_{11}\mathrm{e}^{\lambda_2\xi} + c_{12}\mathrm{e}^{\lambda_3\xi}, & \Delta + \tau_s \le \xi < \infty, \end{cases} \tag{15}$$

$$V(\xi) = LI_\xi(\xi) + rI(\xi), \tag{16}$$

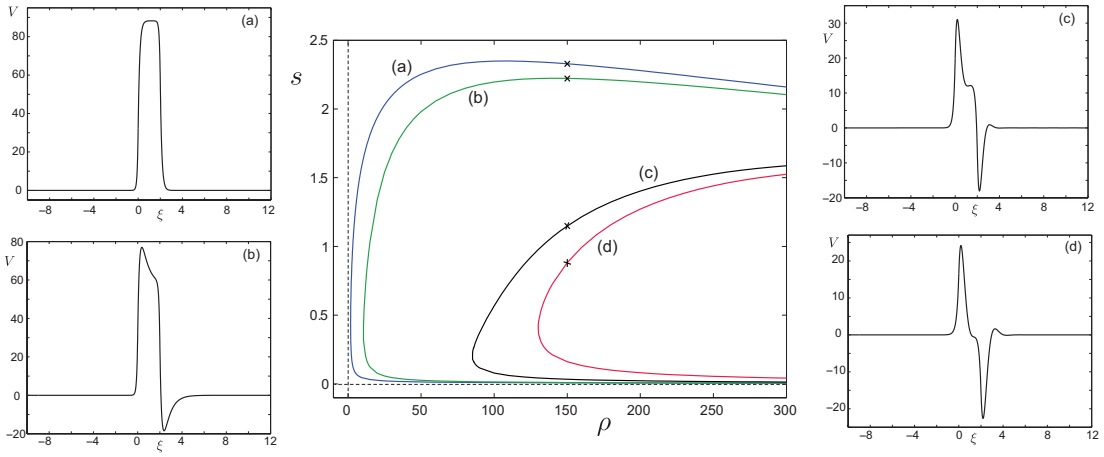

FIG. 3. Speed of a travelling pulse as a function of spine density ρ. (a) Passive membrane ($r \to \infty$), (b) $r = 0.1$, $L = 0.1$, (c) $r = 0.01$, $L = 0.01$ and (d) $r = 0.001$, $L = 0.01$.The profiles of travelling pulses are shown for $\rho = 150$ and (a) $s = 2.3291$, (b) $s = 2.2226$, (c) $s = 1.1490$, and (d) $s = 0.8818$. Other parameters are as in Figure 2, $h = 0.25$, $\widehat{C} = 1$, $\widehat{r} = 1$.

and the unknown coefficients $c_1, \ldots, c_{12}$ may be found from the continuity conditions at $\xi = 0$, $\xi = \tau_s$, $\xi = \Delta$ and $\xi = \Delta + \tau_s$. It is also straightforward to modify equation (15) for Case II when two of the eigenvalues are complex (given in Appendix A2) and the unknown coefficients may also be found by requesting the continuity of solutions at each interval of ξ. The speed of a travelling double pulse can be found by demanding that the spine head reaches the threshold at $\xi = 0$ and $\xi = \Delta$. Here we assume a simple refractory mechanism whereby the function $U(\xi)$ is held at the reset level $U_{\text{res}} = 0$ for a time τ_s after a spiking event. Then the speed can be found by simultaneously solving the following system of equations for unknown s and Δ:

$$h = \frac{1}{\widehat{C} r_s} \int_{-\infty}^{0} V(\xi') \mathrm{e}^{\varepsilon_0 \xi'} \mathrm{d}\xi', \tag{17}$$

$$h = \frac{\mathrm{e}^{-\varepsilon_0 \Delta}}{\widehat{C} r_s} \int_{\tau_s}^{\Delta} V(\xi') \mathrm{e}^{\varepsilon_0 \xi'} \mathrm{d}\xi'. \tag{18}$$

After integration equation (17) has the same form as equation (14). The integral in (18) can also be found for both Case I and Case II. For example, for real λ_i equation (18) takes

the form

$$h = \frac{1}{\widehat{C}r_s}\left[\frac{c_5(\mathrm{e}^{\lambda_1\Delta} - \mathrm{e}^{\lambda_1\tau_s+\varepsilon_0(\tau_s-\Delta)})(L\lambda_1 + r)}{\lambda_1 + \varepsilon_0} + \frac{c_6(\mathrm{e}^{\lambda_2\Delta} - \mathrm{e}^{\lambda_2\tau_s+\varepsilon_0(\tau_s-\Delta)})(L\lambda_2 + r)}{\lambda_2 + \varepsilon_0}\right.$$
$$\left. + \frac{c_7(\mathrm{e}^{\lambda_3\Delta} - \mathrm{e}^{\lambda_3\tau_s+\varepsilon_0(\tau_s-\Delta)})(L\lambda_3 + r)}{\lambda_3 + \varepsilon_0}\right] \tag{19}$$

(see Appendix A2 for λ_i from Case II). Figure 4A shows the speed of a double pulse as a function of spine density ρ for the parameters $r = 0.001$ and $L = 0.01$ (solid black curve). In the same figure we plot the speed of a solitary pulse for the same parameters (dashed red curve). Speeds of the single and double pulses are very similar to each other (see the inner plot in this figure). This can be explained by Figure 4B that shows the period Δ as a function of ρ. The values of Δ are reasonably large and thus the two pulses only interact weakly. Figures 4C and D show the profiles of the slow and fast waves respectively when $\rho = 140$.

For studying a periodic travelling wave we consider the firing times $T^m(x) = x/s + (m-1)\Delta$ with $m = 1,\ 2, \ldots$. Then the solution to (6)–(7) with real λ_i (Case I) takes the form

$$I(\xi) = \begin{cases} c_1\mathrm{e}^{\lambda_1\xi} + c_2\mathrm{e}^{\lambda_2\xi} + c_3\mathrm{e}^{\lambda_3\xi} + Q, & 0 \le \xi \le \tau_s, \\ c_4\mathrm{e}^{\lambda_1\xi} + c_5\mathrm{e}^{\lambda_2\xi} + c_6\mathrm{e}^{\lambda_3\xi}, & \tau_s \le \xi \le \Delta, \end{cases} \tag{20}$$

$$V(\xi) = LI_\xi(\xi) + rI(\xi), \tag{21}$$

and the unknown coefficients $c_1, \ldots, c_6$ may be found from the continuity and periodicity of the solutions. The form of solution (20) for Case II is given in Appendix A3. Figure 5 demonstrates an example of a periodic travelling wave for some chosen set of parameters. The self-consistent speed of such a wave can be determined by demanding that the IF process in the spine head reaches the threshold at $\xi = \Delta$, i.e from the condition $U(\Delta) = h$. This condition leads to equation (18) which implicitly defines a dispersion relationship $s = s(\Delta)$ giving the wave speed s as a function of the period Δ. In the limit $r \to \infty$ these results recover the results obtained by Coombes in [13] for the SDS model with a passive dendritic cable. Figure 6 shows an example of a dispersion curve in our model. One may notice an oscillatory behaviour in the upper and lower branches of the dispersion curve. For a better view magnified plots of the areas marked by rectangles are shown in Figures 6A and B. These oscillations arise from the resonant nature of the dendritic membrane

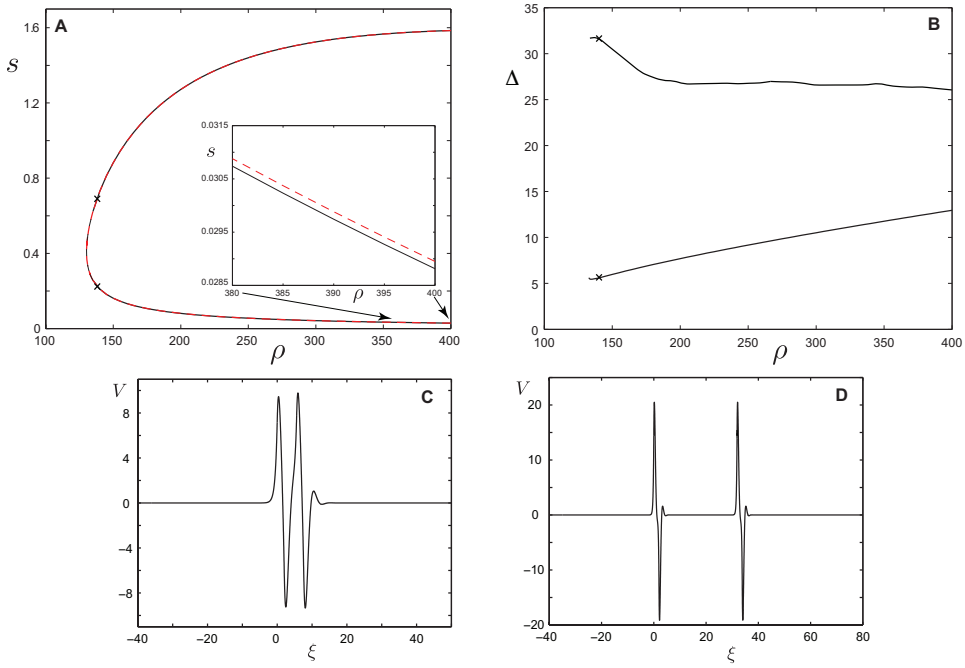

FIG. 4. **A**: Speed of a double pulse (black curve) and a solitary pulse (dashed red curve) as a function of spine density ρ. The inner plot is a magnified view of a part of the lower branch when ρ is between 380 and 400. **B**: Period Δ of a double pulse as a function of spine density ρ. **C** and **D**: Two profiles of double pulses when $\rho = 140$ (indicated by crosses in **A** and **B**). Parameters: $r = 0.001$, $L = 0.01$, $U_{\text{res}} = 0$, $\tau_R = \tau_s$, (**C**) $s = 0.2104$, $\Delta = 5.5907$, (**D**) $s = 0.7292$, $\Delta = 31.858$. Other parameters are as in Figure 3.

and they become more pronounced as $r \to 0$. The stability of the periodic travelling wave can be determined using a kinematic theory (given in Appendix B) that indicates that the solution of the system is stable if the gradient of the dispersion curve is positive, i.e. $s'(\Delta) > 0$. Thus, the oscillatory nature of the dispersion curve leads to alternating regions of stable (positive gradient, solid line) and unstable (negative gradient, dashed line) periodic travelling waves. A similar type of a dispersion curve, but with oscillations only present in the upper branch, has been earlier observed in [26] for a continuum model of synaptically interacting IF neurons after taking into account filtering properties of resonant dendrites. The oscillatory behaviour of both upper and lower branches of the dispersion curve in our model indicates the existence of parameter regions where the fast and slow stable periodic travelling waves coexist.

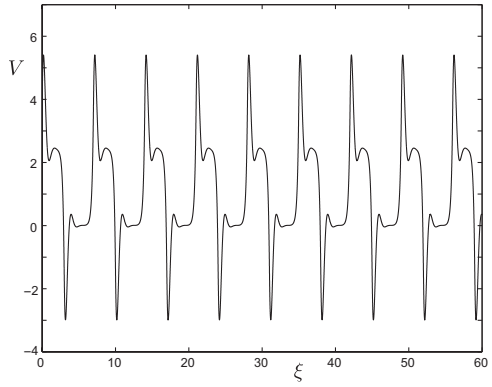

FIG. 5. An example of a periodic travelling wave in the model of a resonant cable with active spines for the following parameters: $r = 0.01$, $L = 0.008$, $\rho = 25$, $s = 1$, $\Delta = 7$, $\tau_s = 3$. Other parameters are as in Figure 2.

This mathematical treatment for studying periodic travelling waves may be naturally extended to waves of multiple periodicity. For example, a double periodic wave can be studied by introducing two periods Δ_1 and Δ_2 ($\Delta_1 < \Delta_2$) and considering that during one periodic cycle the firing events from the spine head at position x occur at the firing times x/s, $x/s + \Delta_1$ and $x/s + \Delta_2$. As shown in [26] the solutions of multiple periodic waves may branch from the stationary points of the dispersion curve (the points of changes in stability).

IV. DISCRETE LIMIT

In this section we consider the case of a discrete distribution of spines. We assume that spines are connected to the cable at the discrete points x_n with the distribution function $\rho(x)$ in (1) given by $\rho(x) = \sum_{n\in\Gamma} \delta(x - x_n)$, where Γ is a discrete set that indexes the spines. This model can be solved using an approach recently developed in [24]. Let us use the notation $I_{\rm sp}(x,t)$ for the total current that is passed into the cable from all active spines, i.e. $I_{\rm sp}(x,t) = \rho(x)(\widehat{V} - V)/r_s$. Introducing the Laplace transform with spectral parameter ω

$$\mathcal{L}[f(t)] = \widetilde{f}(\omega) = \int_0^\infty f(t)\mathrm{e}^{-\omega t}\mathrm{d}t, \tag{22}$$

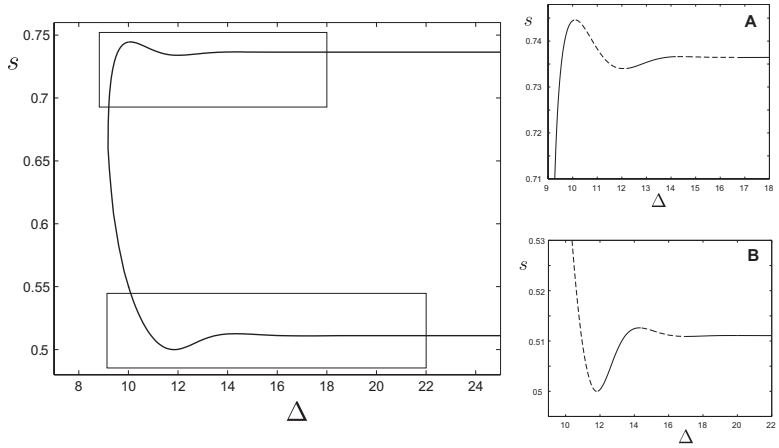

FIG. 6. Dispersion curve $s = s(\Delta)$ of the periodic travelling wave for the following parameters: $\rho = 25$, $r = 0.001$, $L = 0.07$, $h = 0.26$, $U_{\text{res}} = 0$, $\tau_R = \tau_s$. Other parameters as in Figure 3. **A** and **B**: Magnified views of two parts of the dispersion curve indicated by rectangles. Solid (dashed) line corresponds to the stable (unstable) solution.

and applying it to equations (1)-(2) with the initial conditions $V(x,0) = 0$ and $I(x,0) = 0$ we obtain the following ODE

$$-\widetilde{V}_{xx} + \gamma^2(\omega)\widetilde{V} = \frac{\widetilde{I}_{\text{sp}}}{CD}, \tag{23}$$
$$\gamma^2(\omega) = \frac{1}{D}\left[\frac{1}{\tau} + \omega + \frac{1}{C(r+\omega L)}\right],$$

where $\widetilde{V} = \widetilde{V}(x,\omega)$ and $\widetilde{I}_{\text{sp}} = \widetilde{I}_{\text{sp}}(x,\omega)$. A new re-scaled space $X = \gamma(\omega)x$ can be introduced here and equation (23) then takes the form

$$-\widetilde{V}_{XX} + \widetilde{V} = \frac{\widetilde{I}_{\text{sp}}(X/\gamma(\omega),\omega)}{CD\gamma^2(\omega)}. \tag{24}$$

Using the Green's function $\mathrm{e}^{-|X|}/2$ of the operator $(1 - \mathrm{d}_{XX})$ on an infinite domain, we may write the general solution to (24) in the following form:

$$\widetilde{V}(X,\omega) = \int_{-\infty}^{\infty} \frac{\mathrm{e}^{-|X-Y|}}{2} \frac{\widetilde{I}_{\text{sp}}(Y/\gamma(\omega),\omega)}{CD\gamma^2(\omega)} \mathrm{d}Y. \tag{25}$$

We introduce the function

$$\widetilde{G}(x,\omega) = \frac{\mathrm{e}^{-\gamma(\omega)|x|}}{2D\gamma(\omega)}, \tag{26}$$

and then in original coordinates the solution (25) takes the form

$$\widetilde{V}(x,\omega) = \frac{1}{C}\int_{-\infty}^{\infty} \widetilde{G}(x-y,\omega)\widetilde{I}_{\rm sp}(y,\omega)\mathrm{d}y. \tag{27}$$

Performing the inverse Laplace transform $\mathcal{L}^{-1}[\widetilde{f}(\omega)]$ defined by the Bromwich integral

$$\mathcal{L}^{-1}[\widetilde{f}(\omega)] = f(t) = \frac{1}{2\pi i}\int_{c-i\infty}^{c+i\infty} \widetilde{f}(\omega)\mathrm{e}^{\omega t}\mathrm{d}\omega \tag{28}$$

to equation (27) we get

$$V(x,t) = \frac{1}{Cr_s}\sum_{k\in\Gamma}\int_0^t G(x-x_k,t-t')[\widehat{V}(x_k,t') - V(x_k,t')]\mathrm{d}t', \tag{29}$$

where $G(x,t) = \mathcal{L}^{-1}[\widetilde{G}(x,\omega)]$ is the Green's function of the infinite resonant dendrite. Here k is the index of spines that have fired. Note that in the limit $r \to \infty$ we get $\gamma^2(\omega) = (1/\tau + \omega)/D$ and recover the original SDS model with purely passive dendritic cable and the Green's function

$$G(x,t) = \frac{1}{\sqrt{4\pi D t}}\mathrm{e}^{-x^2/(4Dt)-t/\tau}\Theta(t), \tag{30}$$

as studied in [14–16].

The implicit equation for the dendritic voltage (29) has a Dyson-like form suggesting a Neumann series solution that can be obtained by repeated substitution of (29) into itself [15, 27, 28]. The spine neck resistance r_s is typically large in biophysical units (in the range of $5 - 150$ MΩ in [29] or even larger as shown for example in [30, 31]). This leads to the contributions of the second- and higher-order terms in the series expansion becoming negligible and allows us to approximate the solution for the voltage by just the first term in equation (29) (see [15, 28] for more discussion). Thus, assuming that each spine is allowed to fire only once we have

$$V(x,t) = \frac{1}{Cr_s}\sum_{k}\int_0^t G(x-x_k,t-t')\eta(t'-T_k)\mathrm{d}t', \tag{31}$$

where the firing times are $T_k = T^1(x_k)$ as defined by (4). These firing times for the construction of solution (31) may be found from the set of threshold conditions $U(x_n,t) \equiv U_n(t) = h$, $n \in \Gamma$, with $U_n(t)$ obtained by integrating (5) with the initial conditions $U_n(0) = 0$. In particular, to find a new firing time $T_{k+1} > \max_k\{T_k\}$ we have to solve the set of threshold conditions for the functions

$$U_n(t) = \frac{1}{\widehat{C}r_s}\int_0^t \mathrm{e}^{\varepsilon_0(t'-t)}V(x_n,t')\mathrm{d}t'. \tag{32}$$

A closed form expression of the Green's function of the resonant dendrite is only present in the Laplace (frequency) domain as equation (26), and for any practical computational implementation the functions $V(x,t)$ and $U_n(t)$ are best represented in Laplace space. For our simple choice of the function $\eta(t) = \eta_0\Theta(t)\Theta(\tau_s - t)$ we have that

$$\widetilde{V}(x,\omega) = \frac{\eta_0}{2DCr_s}\,\frac{1-\mathrm{e}^{-\omega\tau_s}}{\omega\gamma(\omega)}\sum_k \mathrm{e}^{-(\gamma(\omega)|x-x_k|+\omega T_k)} \tag{33}$$

and

$$\widetilde{U}_n(\omega) = \frac{\eta_0}{2DC\widehat{C}r_s^2}\,\frac{1-\mathrm{e}^{-\omega\tau_s}}{\omega\gamma(\omega)(\omega+\varepsilon_0)}\sum_k \mathrm{e}^{-(\gamma(\omega)|x_n-x_k|+\omega T_k)}. \tag{34}$$

By solving the set of threshold conditions $\mathcal{L}^{-1}[\widetilde{U}_n(\omega)] = h$ we obtain a vector of times showing when each spine is able to reach the threshold and identify the smallest time from this vector as a new spiking event. Note that if multiple firing events are not considered, the number of equations in the set of threshold conditions can be reduced by ignoring the spines that have already fired. As a result of finding a newly fired spine an extra term has to be added into the sum in (34) and the same routine is then repeated to obtain subsequent firing events. Once the firing times are determined the solution $V(x,t)$ can be easily constructed by using (33) and performing $\mathcal{L}^{-1}[\widetilde{V}(x,\omega)]$.

In Figure 7 we show a space-time density plot of $V(x,t)$ in our model with 40 spines that are regularly separated with spine spacing d. The wave is initiated from a single active spines at the location $x = 0$ at time $t = 0$ and it propagates in a saltatory manner with a large increase in voltage just after an individual firing event. The presence of a resonant membrane results in oscillations in the tail of this wave. These oscillations can be better seen in Figures 8 and 9 that show examples of voltage profiles as functions of time and space respectively. In Figure 8 we plot $V(x,t)$ at the locations of spine 15 and spine 16 along the cable. Figure 9A shows an example of the voltage profile as a function of space for the time $T_{25} = 9.6667$ (when spine 25 fires) and the time $T_{25} + \tau_s$. A part of this figure indicated by a dashed rectangle is magnified in Figure 9B.

For the case of regular distribution of spines $x_n = nd$, the firing times occur at regular intervals $T_n = n\Delta$, where Δ measures the time between successive threshold crossings at adjacent spine heads. Although a solitary wave in the discrete model travels with a non-constant profile as shown in Figure 7, the speed of this wave is well defined as $s = d/\Delta$.

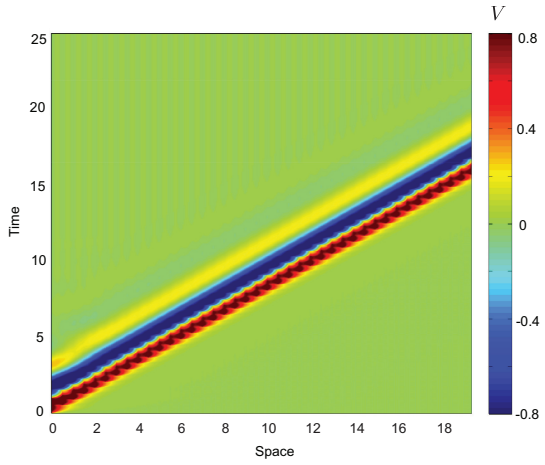

FIG. 7. An example of a travelling wave in the model of a resonant cable with a discrete distribution of active spines for the following parameters: $D = 1$, $\tau = 1$, $\eta_0 = 4$, $r_s = 1$, $\widehat{r} = 1$, $\widehat{C} = 2.5$, $\tau_s = 1$, $h = 0.05$, $r = 0.001$, $L = 0.1$, spine spacing $d = 0.4805$.

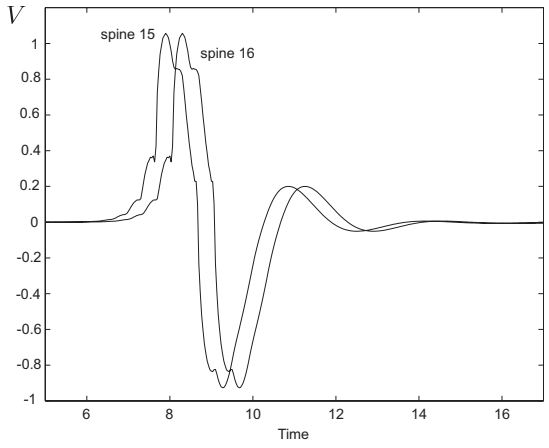

FIG. 8. An example of the voltage profile as a function of time for spine 15 (at $x = 6.727$) and spine 16 (at $x = 7.2075$) along the cable. The parameters are as in Figure 7.

This speed may be determined in a self-consistent manner [14, 15] by the implicit equation $\lim_{n\to\infty} U(nd, n\Delta) = h$, which gives

$$\mathcal{L}^{-1}\left[\frac{1-\mathrm{e}^{-\omega\tau_s}}{\omega\gamma(\omega)(\omega+\varepsilon_0)}\sum_{n=1}^{\infty}\mathrm{e}^{-(\gamma(\omega)nd+\omega n\Delta)}\right] = \frac{2DC\widehat{C}r_s^2}{\eta_0}\,h. \tag{35}$$

In Figure 10 we plot the speed s as a function of distance between the spines for two different sets of parameters r and L. In each case waves fail to propagate if the spines

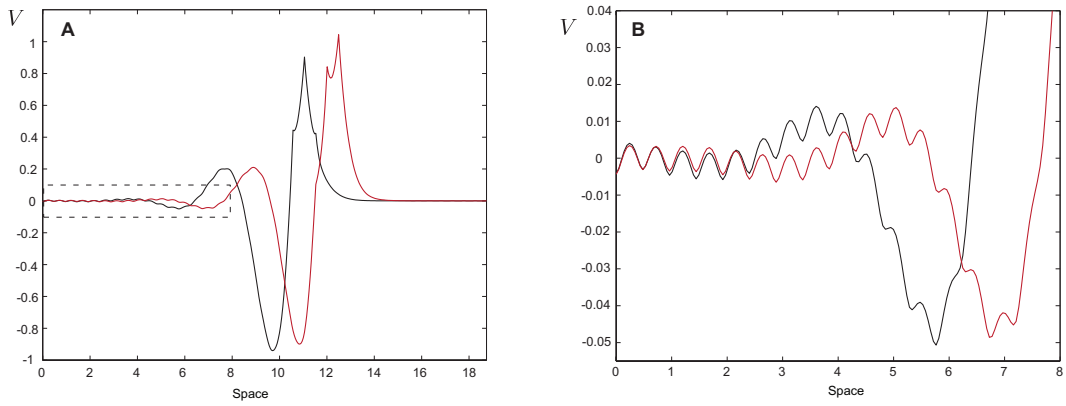

FIG. 9. **A**: An example of the voltage profile as a function of space for the time of firing of spine 25 ($T_{25} = 9.6667$, black curve) and the time $T_{25} + \tau_s$ (red curve). The parameters are as in Figure 7. **B**: A magnified view of the part of **A** indicated by a dashed rectangle.

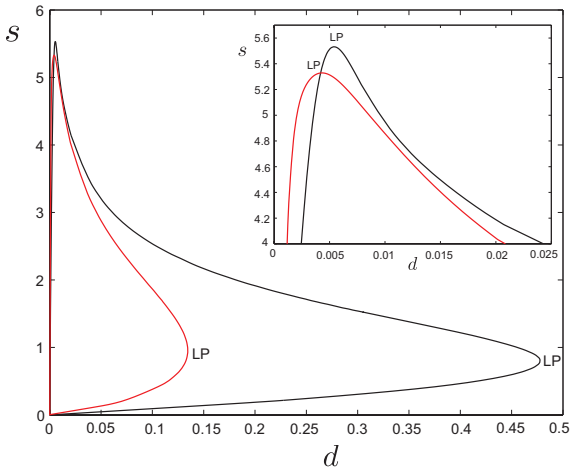

FIG. 10. Speed of a solitary saltatory wave in the model of resonant membrane with active spines for $r = 0.001$, $L = 1$ (black curve) and $r = 0.0001$, $L = 0.1$ (red curve). Other parameters are as in Figure 7. The inner plot is a magnified view of parts of the speed curves showing the limit points for s.

are separated beyond some critical value (to the right of limit point LP). By generalising the stability analysis in [32] it is possible to establish that, as in the continuum model, the faster of the two branches is stable. The inner plot in this figure is a magnified view for small spine spacing, and it demonstrates that the speed of the wave attains its maximum

for small d. Varying only resonant properties of a dendritic cable it is possible to obtain a range of maximum speeds that the system is able to support. Note that these maximum speeds are reached for different values of spine spacing d in each case. This discrete model can be further extended to allow multiple spiking events from individual spines as shown in [15]. In the next section we demonstrate how this model can be generalised to arbitrary dendritic geometries relevant to real neurons.

V. BRANCHED DENDRITIC STRUCTURES

Let us consider an arbitrary branched dendritic structure with a discrete distribution of active spines that are connected to each branch (see Figure 11). The dynamics for the

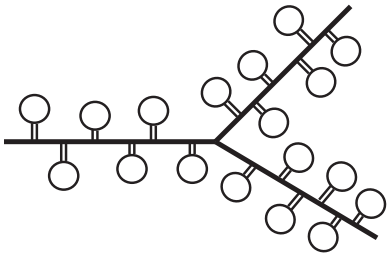

FIG. 11. Schematic diagram of a dendritic tree with active spines.

membrane voltage $V_i(x,t)$ and the resonant current $I_i(x,t)$ with local spatial coordinate x on each branch i are given by equations (1)–(2). The branching structure also requires specifying the appropriate boundary conditions at all nodes (points where branches connect) and terminals (nodes without connections), and these are the continuity of potential and the conservation of current. Assuming that $V_i(x,0) = 0$ and $I_i(x,0) = 0$ for all branches, the voltage on each branch can be found as

$$V_i(x,t) = \frac{1}{Cr_s} \sum_j \sum_{k_j} \int_0^t G_{ij}(x, x_{k_j}, t-t')\eta(t' - T_{k_j})\mathrm{d}t', \tag{36}$$

where k_j indexes the kth spine on branch j and $G_{ij}(x, x_{k_j}, t)$ is the Green's function of the given branching structure. This function can be constructed using the "sum-over-trips" approach developed by Abbott *et al.* [25] for passive dendrites, in particular its recent generalisation by Coombes *et al.* [24] to account for resonant properties of the dendritic

membrane. The function $\widetilde{G}_{ij}(x, y, \omega) = \mathcal{L}[G_{ij}(x, y, t)]$ can be found in terms of the Green's function $\widetilde{G}(x, \omega)$ of an infinite resonant dendrite (equation(26)) as follows

$$\widetilde{G}_{ij}(x, y, \omega) = \sum_{\text{trips}} A_{\text{trip}}(\omega)\widetilde{G}(L_{\text{trip}}(i, j, x, y, \omega), \omega), \tag{37}$$

with an infinite number of trips of length L_{trip} and trip coefficients A_{trip}. We refer the reader to [24] for complete details. Following our earlier approach for an infinite cable the firing times T_{k_j} can be found by solving the set of threshold conditions $U_{n_j}(t) \equiv \mathcal{L}^{-1}[\widetilde{U}_{n_j}(\omega)] = h$ for each branch, where the dynamics U_{n_j} for each spine head is given by (5). The solution $V_i(x, t)$ can then be computed using the Laplace transform representations of the functions $G_{ij}(x, y, t)$ and $\eta(t)$ in (36) to find $\widetilde{V}_i(x, \omega)$ and finally performing $\mathcal{L}^{-1}[\widetilde{V}_i(x, \omega)]$.

We now consider an example of a neural geometry with 24 branches as shown in Figure 12. The spines are distributed along each branch with the average spine spacing of 10 μm. The biophysical parameters across the tree are considered to be the same except for the diffusion coefficients that vary from branch to branch. We assume that one spine at the

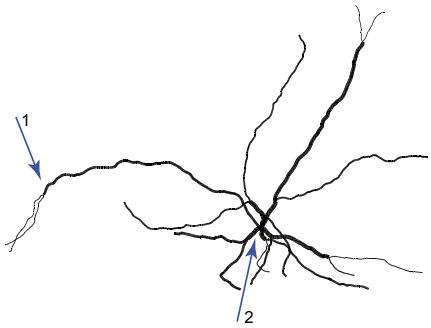

FIG. 12. An example of neural geometry with 24 dendritic branches. Arrow 1 indicates the location of one spine with a low threshold level h. Arrow 2 indicates the location in the tree for which the voltage profiles are shown in Figure 13. Morphology obtained from http://www.koki.hu/~gulyas/ca1cells/cellfiles.htm

location indicated by arrow 1 in Figure 12 has a lower threshold level for the IF mechanism in its spine head than other spines and is easily able to generate repetitive spikes. In Figure 13 we plot the membrane voltage as a function of time measured at the location indicated by arrow 2 in Figure 12. Examples of the voltage profiles are shown for the system with purely passive dendrites (Figure 13A) and for the system with resonant membrane and two

different choices for the inductance L (Figures 13B and C). Varying only the properties of the resonant membrane we are able to observe different patterns of firing in the model. Three snapshots with the neural geometry in Figure 13 demonstrate the membrane voltage in each of these cases at time $t = 50$ ms.

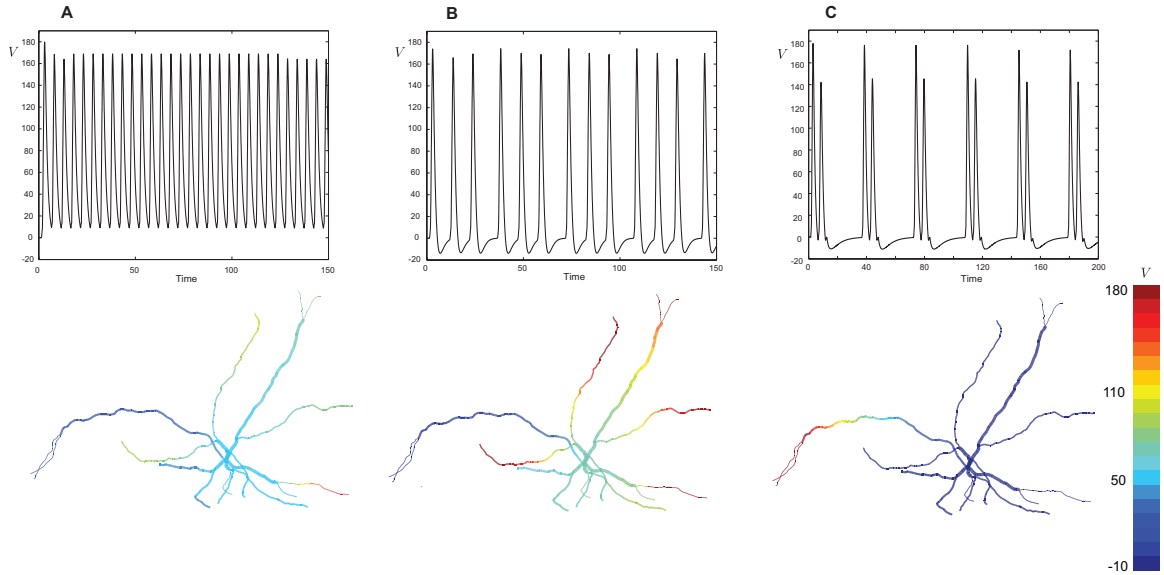

FIG. 13. Top: Examples of the voltage profiles at the location indicated by arrow 2 in Figure 12. Bottom: Snapshots of the membrane voltage across the tree at time $t = 50$ ms. Parameters: $C = 1$ μF/cm^2, $\tau = 1$ ms, diffusion coefficients vary from branch to branch, $r_s = 400$ MΩ, $\eta_0 = 40$ mV, $\tau_s = 1$ ms, $\tau_R = 5$ ms, $\widehat{r} = 4.5$, $\widehat{C} = 0.0001$, $h = 0.05$, $U_{\text{res}} = 0$. **A**: passive membrane ($r \to \infty$), **B**: $r = 2000\ \Omega\ \text{cm}^2$, $L = 6$ H cm^2, **C**: $r = 2000\ \Omega\ \text{cm}^2$, $L = 20$ H cm^2.

VI. DISCUSSION

In this paper we introduced a generalised version of the SDS model by assuming that the active spines are distributed along a resonant dendritic structure. This generalisation allows us to investigate the implication of excitable channels in the spine-head membrane together with resonant channels in the dendrites for single neuron dynamics. The focus of this paper was on both continuous and discrete distributions of spines. Since the resonant dendrites are modelled by a quasi-active (linearised active) membrane and the nonlinear

properties of excitable spines are mimicked by the threshold dynamics the model is mathematically tractable. We showed how travelling wave solutions can be explicitly constructed in our model and how the speed of such waves can be studied as a function of important system parameters. We also demonstrated that this model can be naturally extended to a branched dendritic structure. Importantly, this theoretical framework obviates the need for the numerical solution of the underlying set of PDEs. The voltage response across a dendritic tree can be found in terms of the Green's function that has to be computed only once for a given dendritic structure. As we illustrated here the variation of the resonant properties of the neural membrane in the same system might lead to completely different patterns of firing activities. In real cells, action potentials propagate through the dendritic tree in a complex way and this propagation will depend on action potential initiation (in the axon leading to action potential backpropagation or in the dendrites generating dendritic spikes). Such waves are believed to serve a number of functions, for example to induce synaptic plasticity and to contribute to synaptic integration (more discussion on that can be found in [33]).

Our study does not cover tapered dendrites, and in its current form this framework can be applied to a tapered branch only by approximating the branch by a set of short segments of constant diameters. However, an introduction of exponential tapering leads to the underlying PDE model which is linear (see [34] for a recent discussion of tapering) suggesting that the "sum-over-trips" formalism may be extended to cover this case. Another natural extension of this work would be to obtain a minimal soma-tree model by coupling a branched dendritic tree to a soma. It is relatively straightforward to construct the Green's function for the case of a linear soma model as shown in [24]. An incorporation of an active soma is a substantially harder challenge, however some progress may be achievable by using piece-wise linear models of active membrane.

The way in which neurons respond to spatio-temporal patterns of synaptic inputs depends, to a large extend, on the properties and densities of voltage-gated ion channels. Narayanan and Johnston [35] for example have recently demonstrated that the spatial gradient of h channel density produces a resonance frequency map in dendrites which generates different filtering behaviour for inputs in different regions. Our theoretical framework is practical in use with real neural geometries, in particular when these geometries are sup-

plemented with data governing the distribution of active ionic conductances. In the case of channels responsible for sub-threshold resonance properties of neurons, access to dual potential recording data will allow one to recover the quasi-active properties of dendrites using the theory and algorithms developed by Cox and Griffith [36]. Our model can then be used for a more systematic exploration of the way in which the biophysical properties of individual branches contribute to the overall response at the level of the whole tree.

Dendritic spines are highly dynamic structures that are also known to have significant impact on neuronal processes and are particularly critical for local signal integration and molecular compartmentalisation [37]. The notion of discrete dendritic spines in the model allows us to attribute individual biophysical parameters (that can be dynamic) to groups of spines depending on their locations on a dendritic tree. Experimental observations also indicate that synaptic efficacy scales with distance from the soma [38], a characteristic that is often referred to as "dendritic democracy". This phenomenon has been earlier explored from a theoretical perspective in a passive model of a dendritic tree [28]. Recent experimental and computational studies of Katz *et al.* [39] show that the synapses are scaled in the direction of normalising the contribution of individual inputs to dendritic spikes in CA1 pyramidal neurons. It would be useful to extend [28] and investigate democracy in the presence of active conductances within the framework we have presented here.

Although new experimental technologies for studying dendrites have significantly advanced in recent years, there is as yet little understanding of the specific structure–function relationships between channel densities and local geometry. Thus, working within this extended theoretical framework allows us to improve our understanding of how the presence of ion channels combined with the complexity of dendritic geometries can influence single neuron computation. In addition, a minimal computationally fast soma-tree model based on the extension of this framework might be a good candidate for studying networks of spatially extended neurons.

ACKNOWLEDGEMENTS

I would like to thank S Coombes for the helpful discussions during the completion of this work. I would also like to acknowledge the support provided by an RCUK fellowship.

APPENDIX

A1. Single pulse, Case II

Defining the solutions for $I(\xi)$ and $V(\xi)$ on each interval of ξ by $I_i(\xi)$ and $V_i(\xi)$, $i = 1, \ldots, 3$, the continuity conditions yield the following set of equations:

$$I_1(0) = I_2(0), \quad I_2(\tau_s) = I_3(\tau_s), \quad V_1(0) = V_2(0),$$

$$V_2(\tau_s) = V_3(\tau_s),\ V_{1\xi}(0) = V_{2\xi}(0),\ V_{2\xi}(\tau_s) = V_{3\xi}(\tau_s).$$

Then the coefficients $\overline{c}_1, \ldots, \overline{c}_6$ can be found from the system of linear equations $\mathbf{AC} = \mathbf{B}$, where

$$\mathbf{C} = (\overline{c}_1, \overline{c}_2, \overline{c}_3, \overline{c}_4, \overline{c}_5, \overline{c}_6)^{\mathrm{T}}, \qquad \mathbf{B} = (Q, -Q, rQ, -rQ, 0, 0)^{\mathrm{T}},$$

and the elements of matrix $\mathbf{A}$, namely a_{ij}, are defined as follows

$$a_{11} = 1,\ a_{12} = -1,\ a_{13} = -1,\ a_{14} = 0,\ a_{15} = 0,\ a_{16} = 0,$$

$$a_{21} = 0,\ a_{22} = \mathrm{e}^{\lambda_1\tau_s},\ a_{23} = \mathrm{e}^{\alpha\tau_s}\cos(\beta\tau_s),\ a_{24} = \mathrm{e}^{\alpha\tau_s}\sin(\beta\tau_s),\ a_{25} = -a_{23},\ a_{26} = -a_{24},$$

$$a_{31} = L\lambda_1 + r,\ a_{32} = -a_{31},\ a_{33} = -(L\alpha + r),\ a_{34} = -L\beta,\ a_{35} = 0,\ a_{36} = 0,$$

$$a_{41} = 0,\ a_{42} = \mathrm{e}^{\lambda_1\tau_s}(L\lambda_1 + r),\ a_{43} = \mathrm{e}^{\alpha\tau_s}[\cos(\beta\tau_s)(L\alpha + r) - L\beta\sin(\beta\tau_s)],$$

$$a_{44} = \mathrm{e}^{\alpha\tau_s}[\sin(\beta\tau_s)(L\alpha + r) + L\beta\cos(\beta\tau_s)],\ a_{45} = -a_{43},\ a_{46} = -a_{44},$$

$$a_{51} = \lambda_1(L\lambda_1 + r),\ a_{52} = -a_{51},\ a_{53} = L(\beta^2 - \alpha^2) - r\alpha,\ a_{54} = -\beta(2L\alpha + r),\ a_{55} = 0,\ a_{56} = 0,$$

$$a_{61} = 0,\ a_{62} = \mathrm{e}^{\lambda_1\tau_s}\lambda_1(L\lambda_1 + r),\ a_{63} = \mathrm{e}^{\alpha\tau_s}[(L\alpha^2 - L\beta^2 + r\alpha)\cos(\beta\tau_s) - (2L\alpha\beta + r\beta)\sin(\beta\tau_s)],$$

$$a_{64} = \mathrm{e}^{\alpha\tau_s}[(L\alpha^2 - L\beta^2 + r\alpha)\sin(\beta\tau_s) + (2L\alpha\beta + r\beta)\cos(\beta\tau_s)],\ a_{65} = -a_{63},\ a_{66} = -a_{64}.$$

A2. Double pulse, Case II

$$I(\xi) = \begin{cases} \overline{c}_1\mathrm{e}^{\lambda_1\xi}, & -\infty < \xi \le 0, \\ \overline{c}_2\mathrm{e}^{\lambda_1\xi} + \mathrm{e}^{\alpha\xi}[\overline{c}_3\cos(\beta\xi) + \overline{c}_4\sin(\beta\xi)] + Q, & 0 \le \xi \le \tau_s, \\ \overline{c}_5\mathrm{e}^{\lambda_1\xi} + \mathrm{e}^{\alpha\xi}[\overline{c}_6\cos(\beta\xi) + \overline{c}_7\sin(\beta\xi)], & \tau_s \le \xi \le \Delta, \\ \overline{c}_8\mathrm{e}^{\lambda_1\xi} + \mathrm{e}^{\alpha\xi}[\overline{c}_9\cos(\beta\xi) + \overline{c}_{10}\sin(\beta\xi)] + Q, & \Delta \le \xi \le \Delta + \tau_s, \\ \mathrm{e}^{\alpha\xi}[\overline{c}_{11}\cos(\beta\xi) + \overline{c}_{12}\sin(\beta\xi)], & \Delta + \tau_s \le \xi < \infty. \end{cases}$$

The unknown coefficients $\overline{c}_1, \ldots, \overline{c}_{12}$ (as well as $c_1, \ldots, c_{12}$ in (15) for Case I) can be found from the equations that ensure the continuity conditions at each interval of ξ:

$$I_1(0) = I_2(0), \quad I_2(\tau_s) = I_3(\tau_s), \quad I_3(\Delta) = I_4(\Delta), \quad I_4(\Delta + \tau_s) = I_5(\Delta + \tau_s),$$

$$V_1(0) = V_2(0), \quad V_2(\tau_s) = V_3(\tau_s), \quad V_3(\Delta) = V_4(\Delta), \quad V_4(\Delta + \tau_s) = V_5(\Delta + \tau_s),$$

$$V_{1\xi}(0) = V_{2\xi}(0), \; V_{2\xi}(\tau_s) = V_{3\xi}(\tau_s), \; V_{3\xi}(\Delta) = V_{4\xi}(\Delta), \; V_{4\xi}(\Delta + \tau_s) = V_{5\xi}(\Delta + \tau_s).$$

Equation (18) for Case II takes the form

$$\begin{aligned} h \;=\; & \frac{1}{\widehat{C} r_s}\Bigg[\frac{\overline{c}_5(\mathrm{e}^{\lambda_1\Delta} - \mathrm{e}^{\lambda_1\tau_s + \varepsilon_0(\tau_s - \Delta)})(L\lambda_1 + r)}{\lambda_1 + \varepsilon_0} \\ & + \; Q_1[\mathrm{e}^{\alpha\Delta}((\alpha + \varepsilon_0)\cos(\beta\Delta) + \beta\sin(\beta\Delta)) - \mathrm{e}^{\alpha\tau_s + \varepsilon_0(\tau_s - \Delta)}((\alpha + \varepsilon_0)\cos(\beta\tau_s) + \beta\sin(\beta\tau_s))] \\ & + \; Q_2[\mathrm{e}^{\alpha\Delta}((\alpha + \varepsilon_0)\sin(\beta\Delta) - \beta\cos(\beta\Delta)) - \mathrm{e}^{\alpha\tau_s + \varepsilon_0(\tau_s - \Delta)}((\alpha + \varepsilon_0)\sin(\beta\tau_s) - \beta\cos(\beta\tau_s))]\Bigg], \end{aligned}$$

where

$$Q_1 = \frac{\overline{c}_6(L\alpha + r) + \overline{c}_7 L\beta}{(\alpha + \varepsilon_0)^2 + \beta^2}, \qquad Q_2 = \frac{\overline{c}_7(L\alpha + r) - \overline{c}_6 L\beta}{(\alpha + \varepsilon_0)^2 + \beta^2}.$$

A3. Periodic wave, Case II

$$I(\xi) = \begin{cases} \overline{c}_1\mathrm{e}^{\lambda_1\xi} + \mathrm{e}^{\alpha\xi}[\overline{c}_2\cos(\beta\xi) + \overline{c}_3\sin(\beta\xi)] + Q, & 0 \le \xi \le \tau_s, \\ \overline{c}_4\mathrm{e}^{\lambda_1\xi} + \mathrm{e}^{\alpha\xi}[\overline{c}_5\cos(\beta\xi) + \overline{c}_6\sin(\beta\xi)], & \tau_s \le \xi \le \Delta. \end{cases}$$

The unknown coefficients $\overline{c}_1, \ldots, \overline{c}_6$ (as well as $c_1, \ldots, c_6$ in (20) for Case I) can be found from the continuity and periodicity of the solution, i.e. by solving simultaneously the following equations:

$$I_1(0) = I_2(\Delta), \quad I_1(\tau_s) = I_2(\tau_s), \quad V_1(0) = V_2(\Delta),$$

$$V_1(\tau_s) = V_2(\tau_s), \; V_{1\xi}(0) = V_{2\xi}(\Delta), \; V_{1\xi}(\tau_s) = V_{2\xi}(\tau_s).$$

B. Kinematic theory

Following [40] the ansatz for periodic travelling waves gives

$$\frac{\mathrm{d}T^n}{\mathrm{d}x} = \frac{1}{s(\Delta^n)}, \qquad \Delta^n(x) = T^n(x) - T^{n-1}(x).$$

For linear stability analysis we consider local perturbations of the firing times as $T^n(x) \to T^n(x)+g^n(x)$. A propagating wave of period Δ is stable if under the perturbation the system converges to the unperturbed solution, i.e. $g^n(x) \to 0$ as $x \to \infty$. Inserting the perturbed solution in the kinematic equation above gives

$$\frac{\mathrm{d}g^n(x)}{\mathrm{d}x} = -\frac{s'(\Delta)}{s^2(\Delta)}[g^n(x) - g^{n-1}(x)].$$

Thus, a linear stability analysis of the kinematic equation shows that a periodic wave solution with period Δ is stable if $s'(\Delta) > 0$.

---

[1] R Cajal. *Histology of the Nervous System of Man and Vertebrates* (trans. N Swanson and L W Swanson). Oxford University Press, New York, 1995 (first published 1899).

[2] T H Brown, E W Kairiss, and C L Keenan. Hebbian synapses: biophysical mechanisms and algorithms. *Annual Review of Neuroscience*, 13:475–511, 1990.

[3] J P Miller, W Rall, and J Rinzel. Synaptic amplification by active membrane in dendritic spines. *Brain Research*, 325:325–330, 1985.

[4] B W Mel, D L Ruderman, and K A Archie. Translation-invariant orientation tuning in visual 'complex' cells could derive from intradendritic computations. *Journal of Neuroscience*, 18:4325–4334, 1998.

[5] M E Larkum, J J Zhu, and B Sakmann. A new cellular mechanism for coupling inputs arriving at different cortical layers. *Nature*, 398:338–341, 1999.

[6] J Shepherd. The dendritic spine: a multifunctional integrative unit. *Journal of Neurophysiology*, 75:2197–2210, 1996.

[7] M Segal. Dendritic spines and long-term plasticity. *Nature Review Neuroscience*, 6:277–284, 2005.

[8] V A Alvarez and B L Sabatini. Anatomical and physiological plasticity of dendritic spines. *Annual Review of Neuroscience*, 30:79–97, 2007.

[9] I Segev and W Rall. Excitable dendrites and spines: earlier theoretical insights elucidate recent direct observations. *Trends in Neurosciences*, 21(11):453–460, 1998.

[10] S M Baer and J Rinzel. Propagation of dendritic spikes mediated by excitable spines: A continuum theory. *Journal of Neurophysiology*, 65(4):874–890, 1991.

[11] G J Lord and S Coombes. Traveling waves in the Baer and Rinzel model of spine studded dendritic tissue. *Physica D*, 161:1–20, 2002.

[12] S Coombes and P C Bressloff. Solitary waves in a model of dendritic cable with active spines. *SIAM Journal on Applied Mathematics*, 61(2):432–453, 2000.

[13] S Coombes. From periodic travelling waves to travelling fronts in the spike-diffuse-spike model of dendritic waves. *Mathematical Biosciences*, 170:155–172, 2001.

[14] S Coombes and P C Bressloff. Saltatory waves in the spike-diffuse-spike model of active dendritic spines. *Physical Review E*, 91:028102, 2003.

[15] Y Timofeeva, G J Lord, and S Coombes. Spatio-temporal filtering properties of a dendritic cable with active spines: A modeling study in the spike-diffuse-spike framework. *Journal of Computational Neuroscience*, 21:293–306, 2006.

[16] Y Timofeeva, G J Lord, and S Coombes. Dendritic cable with active spines: A modelling study in the spike-diffuse-spike framework. *Neurocomputing*, 69:1058–1061, 2006.

[17] D Johnston and R Narayanan. Active dendrites: colorful wings of the mysterious butterflies. *Trends in Neurosciences*, 31(6):309–316, 2008.

[18] S R Williams, S R Christensen, G J Stuart, and M Häusser. Membrane potential bistability is controlled by the hyperpolarization-activated current I_h in rat cerebellar Purkinje neurons *in vitro*. *Journal of Physiology*, 539:469–483, 2002.

[19] A L Hodgkin and A F Huxley. A quantitative description of membrane current and its application to conduction and excitation in nerve. *Journal of Physiology*, 117:500–544, 1952.

[20] A Mauro, F Conti, F Dodge, and R Schor. Subthreshold behavior and phenomenological impedance of the squid giant axon. *Journal of General Physiology*, 55:497–523, 1970.

[21] D Ulrich. Dendritic resonance in rat neocortical pyramidal cells. *Journal of Neurophysiology*, 87:2753–2759, 2002.

[22] E P Cook, J A Guest, Y Liang, N Y Masse, and C M Colbert. Dendrite-to-soma input/output function of continuous time-varying signals in hippocampal CA1 pyramidal neurons. *Journal of Neurophysiology*, 98:2943–2955, 2007.

[23] C Koch. Cable theory in neurons with active, linearized membranes. *Biological Cybernetics*, 50:15–33, 1984.

[24] S Coombes, Y Timofeeva, C-M Svensson, G J Lord, K Josić, S J Cox, and C M Colbert. Branching dendrites with resonant membrane: A "sum-over-trips" approach. *Biological Cybernetics*, 97:137–149, 2007.

[25] L F Abbott, E Fahri, and S Gutmann. The path integral for dendritic trees. *Biological Cybernetics*, 66:49–60, 1991.

[26] M P James, S Coombes, and P C Bressloff. Effects of quasi-active membrane on multiple periodic traveling waves in integrate-and-fire systems. *Physical Review E*, 67(051905), 2003.

[27] P C Bressloff and S Coombes. Physics of the extended neuron. *International Journal of Modern Physics B*, 11:2343–2392, 1997.

[28] Y Timofeeva, S J Cox, S Coombes, and K Josić. Democratization in a passive dendritic tree: an analytical investigation. *Journal of Computational Neuroscience*, 25:228–244, 2008.

[29] K Svoboda, D W Tank, and W Denk. Direct measurement of coupling between dendritic spines and shafts. *Science*, 272:716–719, 1996.

[30] D Tsay and R Yuste. On the electrical function of dendritic spines. *Trends in Neurosciences*, 24(2):77–83, 2004.

[31] B L Bloodgood and B L Sabatini. Neuronal activity regulates diffusion across the neck of dendritic spines. *Science*, 310:866–869, 2005.

[32] S Coombes. The effect of ion pumps on the speed of travelling waves in the fire-diffuse-fire model of Ca^{2+} release. *Bulletin of Mathematical Biology*, 63:1–20, 2001.

[33] N Spruston, G Stuart, and M Häusser. Dendritic integration. In G Stuart, N Spruston, and M Häusser, editors, *Dendrites*. Oxford University Press, New York, 2008.

[34] A Scott. *Neuroscience: A mathematical primer*. Springer, Heidelberg, 2002.

[35] R Narayanan and D Johnston. Long-term potentiation in rat hippocampal neurons is accompanied by spatially widespread changes in intrinsic oscillatory dynamics and excitability. *Neuron*, 56:1061—1075, 2007.

[36] S J Cox and B E Griffith. Recovering quasi-active properties of dendritic neurons from dual potential recordings. *Journal of Computational Neuroscience*, 11:95–110, 2001.

[37] D H Bhatt, S Zhang, and W-B Gan. Dendritic spine dynamics. *Annual Review of Physiology*, 71:261–282, 2009.

[38] J Magee and E Cook. Somatic EPSP amplitude is independent of synapse location in hippocampal pyramidal neurons. *Nature Neuroscience*, 3:895–903, 2000.

[39] Y Katz, V Menon, D A Nicholson, Y Geinisman, W L Kath, and N Spruston. Synapse distribution suggests a two-stage model of dendritic integration in CA1 pyramidal neurons. *Neuron*, 63:171–177, 2009.

[40] R N Miller and J Rinzel. The dependence of impulse propagation speed on firing frequency, dispersion, for the Hodgkin-Huxley model. *Biophysical Journal*, 34:227–259, 1981.